Star formation in merging galaxy clusters

Chiara Ferrari

Intitut für Astrophysik, Universität Innsbruck
Technikerstraße 25, A-6020 Innsbruck
Chiara.Ferrari@uibk.ac.at

Abstract

In the framework of the hierarchical model of structure formation, galaxy clusters form through the accretion and merging of substructures of smaller mass. Merging clusters are a privileged laboratory to test the physics of evolutionary effects on their galaxy members. Shock waves in the ICM driven by the merging event may trigger star formation (Evrard 1991). Other physical mechanisms could trigger star formation within clusters: the infall of galaxies in the high pressure ICM (Dressler & Gunn 1983), the encounters and interactions between galaxies (Lavery & Henry 1988), the rapid variation of the gravitational tidal field (Bekki 1999). On the other side, gas stripping in galaxies due to ram pressure exerted by the ICM could weaken the star-burst phenomenon during cluster collision (Fujita et al. 1999). So far it is not yet clear which one of these competing effects is the dominant one. In this picture, I present the analysis of the dynamical state and star formation properties of the merging cluster Abell 3921 based on the comparison of new optical (Ferrari et al. 2005) and X-ray (Belsole et al. 2005) observations with numerical simulation results.

1 Introduction

In the currently favoured cosmological model (ΛCDM, Ω_m=0.3 and Ω_Λ=0.7), small structures are the first to form, and then they merge giving rise to more and more massive systems in a hierarchical way. Cosmological simulations show that galaxy clusters, which are the most massive gravitationally bound systems of the present Universe, form and evolve through the merging of sub-clusters and groups of galaxies along filamentary structures (e.g. Borgani et al. 2004).

Major cluster-cluster collisions are the most energetic events since the Big Bang, with total releases of gravitational binding energies of the order of 10^{64} ergs (Sarazin 2003). Therefore, the merging event can strongly affect the physical properties of the different cluster components. While in the recent past the effects of mergers on the intra-cluster medium (ICM) and on the internal dynamics of clusters have been analysed in some detail both from the numerical (e.g. Schindler and Böhringer 1993, Schindler and Müller 1993, Ricker & Sarazin 2001) and from the observational point

Reviews in Modern Astronomy 18. Edited by S. Röser
 ISBN 3-527-40608-5

of view (e.g. Davis et al. 1995, Lemonon et al. 1997, Röttiger et al. 1998, Durret et al. 1998, Arnaud et al. 2000, Donnelly et al. 2001, Ferrari et al. 2003), at present the increasing spectral and spatial resolution of both X-ray and optical observations, combined with more and more detailed numerical simulations, open the possibility to analyse the effect of mergers not only on the global cluster properties, but also on the evolution of their galaxies.

The interest in understanding if and how the cluster environment plays a role in the evolution of galaxies begun with the discovery of the so-called "Butcher & Oemler effect". In 1978, Butcher & Oemler reported a strong evolution from bluer to redder colours in cluster galaxies, detecting an excess of blue galaxies at z=0.5 with respect to lower redshift systems. At the beginning of the 80's, Dressler & Gunn pointed out for the first time that the blue colour of the population detected by Butcher & Oemler was the result of star-formation (SF) activity (Dressler & Gunn 1983). Since then, different physical mechanisms have been proposed to be responsible for the triggering and the possible cessation of SF in cluster galaxies. They can be due to the interaction with other galaxies (e.g. mergers and collisions), or to effects specific to the environment, involving either the ICM (e.g. ram-pressure[1] stripping and compression) or the cluster gravitational potential (e.g. tidal effects).

2 Merging clusters: privileged laboratories to test the physics of evolutionary effects

Due to the strong energies involved during cluster-cluster collisions, the merging event can amplify and make the physical mechanisms responsible for the evolution of SF properties in galaxies more efficient. Merging clusters are therefore privileged laboratories to test the physics of evolutionary effects.

Due to the high relative velocities of the colliding sub-clusters ($\approx$3000 km/s), both the ICM density and the relative velocity between the galaxies and the ICM are increased during the merging event. As a consequence, the ram-pressure exerted by the ICM on the galaxy inter-stellar medium (ISM) can significantly increase. Both numerical simulations and observations suggest that the ram-pressure can have a double effect on SF. On one side it can sweep the ISM of galaxies away, thus decreasing their SFR due to a lack of gas. On the other hand, the pressure exerted by the ICM can enhance SF through the compression of the ISM: when gas rich galaxies fall into the central region of a cluster for the first time, they experience a rapid increase of ICM external pressure, quickly exceeding the ISM internal pressure, which triggers the star-burst by compressing the molecular clouds in galaxies (the so-called "first infall" model by Dressler & Gunn 1983). Of course, we could have the same kind of effect whenever a gas rich galaxy moves in a dense ICM with a high relative velocity between them, e.g. during cluster-cluster collisions. Up to now, numerical and observational results have shown that either the ram-pressure stripping (e.g. Fujita et al. 1999, Bartholomew et al. 2001, Gomez et al. 2001), or the ISM com-

[1] $\mathrm{P_{ram} \propto \rho_{ICM} v_{rel}}^2$, where ρ_{ICM} is the density of the inter-cluster medium, and $\mathrm{v_{rel}}$ is the relative velocity between the ICM and the galaxy.

pression (e.g. Dressler & Gunn 1983, Evrard 1991, Poggianti et al. 2004) could be the dominant mechanism acting on SF in galaxy clusters. The two mechanisms can also be both efficient, but with different time scales, since, during the fast infall of a galaxy in a dense ICM, we could have an initial increase and a following drop of SFR (Quilis et al. 2000).

During cluster-cluster collisions, the SF properties of galaxies can also be strongly affected both by tidal effects due to the merging event (Bekki 1999), and by interactions between galaxies (e.g. Lavery & Henry 1988, Bekki, Shioya and Couch 2001). In the first case, the time-dependent tidal gravitational field of the merger gives strong non-axisymmetric perturbations to the disk galaxies in the colliding clusters. Subsequently this tidal field induces an efficient transfer of gas to the central region of the galaxy, and finally triggers the star-burst episode. For what concerns the second point, even if the dense environment of clusters seems to assist galaxy interactions, the effects of collisions between galaxies are weaker in clusters than in the field, since the random velocities of the cluster members are generally greater than the internal velocity dispersions of galaxies (Struck 1999 and references therein). However, if groups of galaxies with a smaller velocity dispersion are falling into major clusters, the effects of interactions may be enhanced. Observational results confirm that a fraction of active galaxies (i.e. with recent or on-going SF) shows significant signs of interactions with other galaxies (e.g. Blake et al. 2005, Zabludoff et al. 1996).

Other mechanisms that have been proposed to affect galaxy properties are: a) "harassment" (Moore et al. 1996), a mechanism that can severely damage the disk of spiral galaxies due to fast (several thousands of km/s) and close encounters with bright galaxies, which can cause impulsive gravitational shocks and a global tidal heating, and b) "strangulation" (or "starvation"), for which a halo of hot gas is stripped from galaxies in dense environments, leading to a gradual winding down of SF as the remaining cold, disk gas is consumed (Larson, Tinsley and Caldwell 1980, Bekki, Couch and Shioya 2002).

In practice, more than one of the above mechanisms is probably responsible for the SF properties of active galaxies in clusters, and in particular in merging clusters, and a general consensus has not yet been reached about the net role played by cluster collisions in the evolution of the SFR.

2.1 Observations and simulations of merging clusters

In this picture, a combined observational and numerical approach is the only way to shed light upon the role played by cluster-cluster collisions on SF. In collaborations with different researchers of several European (Intitut für Astrophysik, Innsbruck, Austria; Observatoire de la Côte d'Azur, Nice, France; INAF, Bologna, Italy; SAp/CEA, Saclay, France), and Australian (Sidney University) institutes, I have begun a multi-wavelength and numerical analysis of a sample of merging galaxy clusters. We aim at investigating which one of the different physical mechanisms summarised in the previous section plays a role in affecting the SFR of cluster galaxies, and at testing if the merging event makes these mechanisms more efficient.

For this we need to determine: a) the dynamical state of the observed galaxy clusters; b) how the star-formation history (SFH) of cluster members varies inside the interacting systems, verifying if there exists a correlation between the spatial distribution of active galaxies and the regions of the cluster mainly affected by the interaction (i.e. characterised by compression and heating of the ICM, and by strong perturbations in the galaxy dynamics); c) evaluate if and how the fraction of active galaxies evolves during the different phases of the merging event. While following all the steps of sub-cluster collisions is in principle feasible from the numerical point of view, it is not possible from the observational side, due to the extremely long time scales of mergers, i.e. several Gyr. We have therefore decided to observe a sample of galaxy clusters going from pre-merging to nearly virialised systems, and to study these clusters by combining optical (imaging: WFI@2.2m ESO, CFH12k@CFHT; spectroscopy: EFOSC2@3.6m ESO, VIMOS@VLT ESO, 2dF@AAT), X-ray (Chandra, XMM) and radio (VLA, ATCA) data.

2.1.1 Observations

In order to fulfil the main objectives of our programme, the observational analysis requires several steps.

- First of all we need to reconstruct very precisely the merging scenario of each observed cluster, determining the mass ratio between the interacting subclusters, their impact parameter, the angle between the collision axis and the plane of the sky, and the time elapsed since the beginning of the interaction. The comparison between optical and X-ray observations is essential for characterising the dynamical state of galaxy clusters. The ICM and galaxy density maps allow us to estimate roughly which phase of the merging event we are observing due to the strong difference in the relaxation time scales of the gas and of the collisionless component in clusters (i.e. galaxies and dark matter). A detailed reconstruction of the merging scenario is then possible through the dynamical and kinematic analysis of member galaxies combined with the study of the density and temperature maps of the ICM (e.g. Arnaud et al. 2000, Maurogordato et al. 2000).

- By combining our optical and radio observations we then identify the active galaxies of the cluster, and we study their velocity and spatial distributions. In order to individuate star-forming and post-star-forming objects, we adopt the classification scheme of Dressler et al. (1999) based on the presence and strength of [OII] emission and Balmer absorption (in particular H_δ) lines in the galaxy spectrum. The objects characterised by the presence of strong Balmer absorption lines and absent [OII] emission are classified as post-starburst (PSB) galaxies. They are often referred to "E+A" or "k+a/a+k" galaxies, since their spectral features are typical of ellipticals with a large population of recently formed A stars. However, the absence of [OII] emission suggests that SF is no longer going on. The conclusion is that these galaxies have previously (<1-1.5 Gyr ago) undergone a burst of SF, which has recently been truncated rather suddenly (Poggianti et al. 1999). The presence of [OII] and,

in general, of emission lines indicates that an episode of SF is going on in the observed galaxy. Following Poggianti et al. (1999), emission line galaxies are normally divided in three categories. Those presenting moderate Balmer absorption and weak to moderate [OII] emission are classified as "e(c)" objects. They have spectra similar to those of typical present-day spirals, but an alternative interpretation is that they could be long star-bursts observed in the late phase of their star-bursting episode. Spectra with very strong [OII] emission are classified as "e(b)" types, and they correspond to star-burst galaxies, since it has been shown that so strong emission lines cannot be reached with a normal spiral-like SFH (Poggianti et al. 1999). Finally, another class of objects has been detected: those with strong Balmer absorption and measurable [OII] emission. Different explanations on the nature of these galaxies have been proposed: they could be PSB galaxies with some residual SF, but, since [OII] emission suffers from strong dust-extinction, they are more likely dusty star-bursts, i.e. e(b)-type galaxies whose strong [OII] emission is obscured by dust. The radio continuum luminosity is on the contrary a tracer of on-going SF that is unbiased by dust (Miller & Owen 2001). Therefore, our radio observations can reveal the presence of star-forming objects, and they can help to disentangle between real post-star forming galaxies and dusty star-forming galaxies. We are also planning to obtain other SFR indicators that are less affected or completely unaffected by dust absorption, i.e. the H_α emission line and IR fluxes.

- Finally, we verify if there exists a link between the presence and the properties of the detected active galaxies and the dynamical state of the cluster. If a correlation is found, we need to compare the observational results to numerical simulations of merging clusters in order to understand which are the physical mechanisms acting on the SFR of cluster galaxies.

2.1.2 N-body and hydrodynamic simulations

Our observational analysis is therefore compared with the numerical results obtained by the HYDRO-SKI team of the Institut für Astrophysik in Innsbruck University (Schindler and collaborators). Combined N-body and hydrodynamic simulations are used to model the massive components of clusters, i.e. dark-matter, galaxies and ICM (van Kampen et al.1999, Domainko et al. 2004, Kapferer et al. 2004).

The comparison of observational results with these simulations is first of all essential to refine the merging scenario reconstructed from the multi-wavelength observations. Secondly it allows to analyse in detail a) which physical mechanisms related to the merging event can affect the SF properties of cluster members, and b) one of the main effects of SF, that is the metal enrichment of the ICM. Since X-ray spectra reveal that the ICM contains metals (Sarazin 1988) and heavy elements are only produced in stars, the processed material must have been ejected by cluster galaxies into the ICM. After SF and subsequent SNs explosions have taken place in cluster members transferring metals to the ISM, the enriched material has to be transported into the ICM. This can happen through different physical mechanisms,

triggered either by the environment, e.g. ram-pressure stripping, or by violent internal processes, e.g. galactic winds developed by massive stars (De Young 1978). The effect of ram-pressure stripping according to the local properties of the ICM, as well as the effect of galactic winds are included in the simulations by Schindler and collaborators. Metallicity is used as a tracer to follow the enriched material, and the simulated metallicity maps can of course be compared to those reconstructed from our X-ray observations.

3 A case study: the merging cluster Abell 3921

In the following I will present our study of the dynamical and SF properties of the merging cluster Abell 3921. These results are based on the analysis of multi-object spectroscopy (EFOSC2@ESO 3.6m) and multi-band (V,R,I) deep imaging (WFI@ESO 2.2m) observations, and are presented in detail in Ferrari et al. (2005). Our optical analysis is compared to the X-ray results of Belsole et al. (2005), based on the XMM observation of A3921.

3.1 Dynamical state of A3921

3.1.1 Optical morphology of A3921

We have investigated the projected spatial morphology of A3921 through several density maps of the galaxy distribution built on the basis of a multi-scale approach. The adopted algorithm is a 2D generalisation of the algorithm presented in Fadda et al. (1998). It involves a wavelet decomposition of the galaxy catalogue performed on five successive scales from which the significant structures are recombined into the final map (following the Eq. [C7] of Fadda et al. 1998). These significant structures are obtained by thresholding each wavelet plane at a level of three times the variance of the coefficients of each plane except for the two smallest scales for which the threshold is increased to four and five times the variance in order to reduce false detections due to the very low mean density of the Poisson process at these scales (0.01 for a chosen grid of 128×128 pixel^2).

In order to avoid possible projection effects, we have isolated galaxies likely to be early types at the cluster redshift on the basis of their colour properties. Indeed, one can notice in the colour magnitude diagram (CMD) of Fig. 1 a well defined red sequence, the characteristic linear structure defined by the bulk of early-type galaxies in a cluster. Finally, from the sample of red sequence galaxies we have additionally excluded galaxies known from spectroscopy not to be cluster members. Fig. 2 shows the resulting red sequence density map at different magnitude cuts (using only galaxies at $\pm1\sigma$ around the red sequence). We can notice that the optical morphology of A3921 is characterised by: a) the presence of several substructures, b) an overall bimodal morphology, with two main clumps (A3921-A and A3921-B), c) an eastern extension of galaxies stronger at faint magnitude cuts, and d) an offset of the Brightest Cluster Galaxy (BCG) from the main density peak of clump A. These results suggest that this system is out of dynamical equilibrium and that it is probably composed of a main cluster interacting with at least two groups, one

to the North-East (clump B) and one to the East, the latter being significantly less luminous than the former.

3.1.2 Dynamical and kinematical properties of A3921

The analysis of the velocity distribution of the cluster members can help us to understand which phase of the merging process we are witnessing. We have therefore performed a kinematical and dynamical analysis of A3921, considering firstly all the confirmed cluster members as a whole dataset (104 galaxies), and secondly the galaxies in the central region of the two main clumps separately (see Fig. 3).

We have applied the statistical indicators of Beers et al. (1990) that give the best estimation of velocity location ("mean") and scale ("dispersion") of a dataset depending on the number of its points. The results are summarised in Table 1. A3921-A and A3921-B show a mean velocity very close to each other and to the whole cluster value, with a velocity offset Δv[2] between the mean velocities of the two clumps of only 89^{+155}_{-177} km/s. Clump A is characterised by the highest velocity dispersion.

Table 1: Properties of the cz distribution for various subsamples of A3921 (Ferrari et al. 2005). $C_{\rm BI}$ and $S_{\rm BI}$ are the mean velocity and the velocity dispersion of the different distributions (biweight estimators for location and scale, Beers et al. 1990)

Subsample	$N_{\rm gal}$	$C_{\rm BI}$ [km/s]	$S_{\rm BI}$ [km/s]
Whole sample	104	28047^{+76}_{-77}	831^{+100}_{-76}
A3921-A	41	28017^{+145}_{-173}	1008^{+156}_{-106}
A3921-B	20	27920^{+88}_{-86}	451^{+215}_{-80}

In dissipationless systems, gravitational interactions of cluster galaxies over a relaxation time generate a Gaussian distribution of their radial velocities; possible deviations from Gaussianity could provide important indications of on-going dynamical processes. We have therefore analysed the velocity distributions of the three sub-samples of Table 1 in order to test the null Gaussian hypothesis. In particular, we have analysed: a) the classical shape estimators of a distribution (skewness and kurtosis, and asymmetry and tail indexes by Bird and Beers 1993), b) 13 1-D statistical tests of Gaussianity included in the ROSTAT package (Beers et al. 1990), c) the improvement in fitting a multiple-component model over a single-one on the velocity distributions of the three samples through the KMM algorithm of McLachlan & Basford (1988), and d) the mean-velocity and velocity-dispersion profiles of

[2]Cosmologically and relativistically corrected from the mean cluster redshift: $\Delta v = c(\bar{z}_A - \bar{z}_B)/(1+\bar{z})$

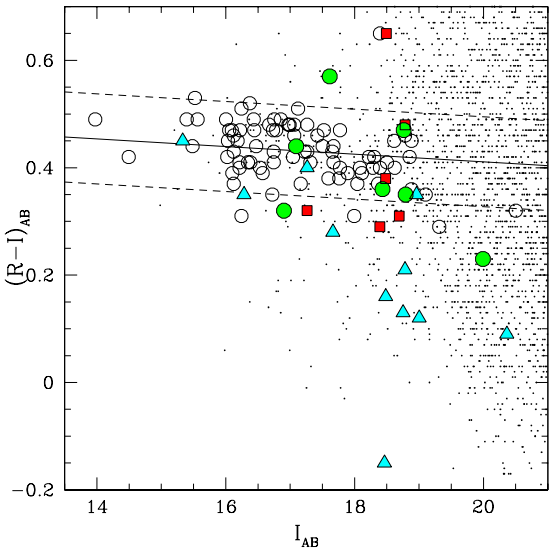

Figure 1: $(R-I)_{\rm AB}$ *vs* $I_{\rm AB}$ colour-magnitude diagrams. All galaxies within 34×34 $\rm arcmin^2$ are shown. Big symbols correspond to confirmed cluster members whereas dots correspond to galaxies without spectroscopic information. Triangles correspond to emission line galaxies, squares to k+a type, circles to galaxies presenting an H-K inversion following the classification described in the text (Sect. 3.2). The solid line is the best linear-fit to the red sequence of the cluster ($(R-I)_{\rm AB} = -0.0071 I_{\rm AB} + 0.5531$, width of $\sigma_{\rm RS}$=0.0837) . The dotted lines are at $\pm 1 \sigma_{\rm RS}$ (Ferrari et al. 2005).

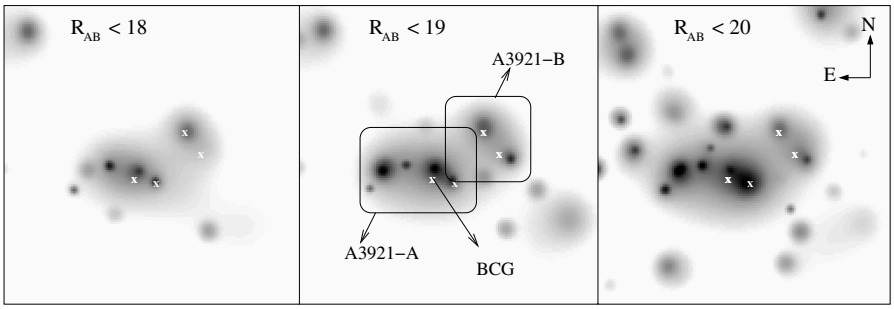

Figure 2: Projected galaxy density maps (using red sequence galaxies without galaxies known not to be cluster members from spectroscopy) on a 34×34 $\rm arcmin^2$ field centred on A3921 and for three magnitude cuts. The white crosses indicate the positions of the four brightest cluster galaxies (Ferrari et al. 2005).

the whole cluster members. The main results of this detailed study suggest that the kinematical properties of the whole sample and of the two sub-clusters do not show strong and clear signatures of merging (see Ferrari et al. 2005 for more details). In particular, the dynamics of the central regions of the two clumps appears to be relatively unaffected by the merging event.

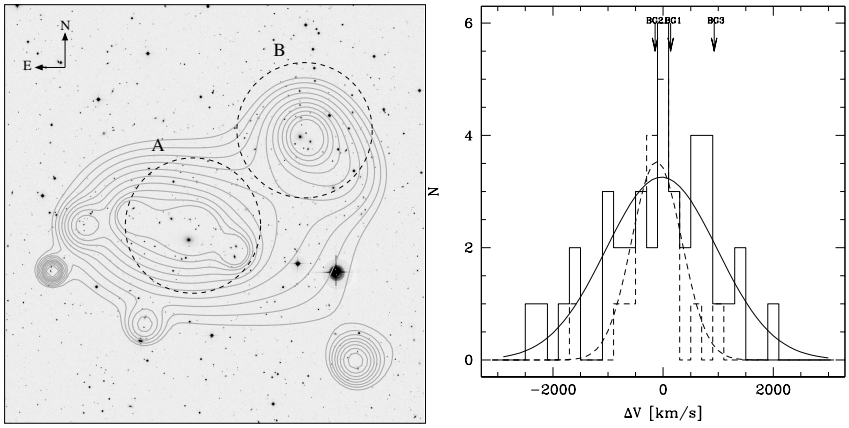

Figure 3: **Left:** Iso-density contours of the projected distribution of the red-sequence galaxies (with $R_{\rm AB} \leq 18$ and after removing galaxies known not to be cluster members from spectroscopic data) superimposed on the central 22×22 $\rm arcmin^2$ of the R–band image of A3921. The dynamical analysis of the two clumps A and B is performed based on the galaxies selected inside the two dashed circles (R$\simeq$ 0.34 Mpc). **Right:** Velocity histogram, with a binning of 200 km/s, of the galaxies in A3921-A (solid line) and in A3921-B (dotted line), according to the division shown in the left panel. The relative Gaussian best–fits to the velocity distributions are superimposed. Arrows show the radial velocities of the three brightest cluster galaxies (Ferrari et al. 2005).

On the basis of the previous results, we have assumed that each sub-cluster is virialized, and we have calculated the mass of A3921-A and A3921-B with the classic virial equation: $M_{\rm vir} = \frac{r_{\rm vir}\sigma^2_{\rm vir}}{G}$, where $\sigma_{\rm vir}$ is the three–dimensional velocity dispersion of the system, and $r_{\rm vir}$ is the virial radius. The results obtained using the pairwise estimator for the viral radius are shown in Table 2 (see Ferrari et al. 2005 for more details).

3.1.3 Conclusions about the dynamical state of A3921

To summarise, in spite of clear merging signatures in the density distribution, the kinematical and dynamical properties both of the whole cluster and of the two subclusters do not show strong signatures of merging. Moreover, the two sub-clusters show very similar mean projected velocities.

Using the observed values of the mass of the two-clumps, their projected spatial separation, and their radial velocity offset, we have applied a two-body dynamical

Table 2: Columns 1 & 2: projected virial radii of A3921-A and A3921-B; columns 3 & 4: virial mass estimates for A3921-A and A3921-B; column 5: mass ratio. Masses are in $10^{14} M_{\odot}$ units and radiii in h^{-1} Mpc units.

$R_{\rm vir}$ (A)	$R_{\rm vir}$ (B)	$M_{\rm vir}$ (A)	$M_{\rm vir}$ (B)	$M_{\rm vir}$ (A) / $M_{\rm vir}$ (B)
0.39 ± 0.02	0.38 ± 0.02	$4.3^{+1.4}_{-1.0}$	$0.8^{+0.7}_{-0.3}$	$5.2^{+4.4}_{-2.5}$

Table 3: Scenarios that could explain the observed dynamical properties of the cluster on the basis of a two-body approach. Col.1: name of the scenario in the text – Col.2: time since last interaction of the two clumps – Col.3: angle between the plane of the sky and the line connecting the centres of the two clumps – Col.4: relative velocity between the two clumps – Col.5: spatial separation between the two systems – Col.6: state of the systems for the possible solutions (Ferrari et al. 2005).

Scenario	T_0 [Gyr]	α [deg]	V [km/s]	R [Mpc]	Solutions
a1	12.6	84.3	89.4	7.5	outgoing
a2	12.6	83.5	89.6	6.5	infalling
a3	12.6	2.2	2318.4	0.7	infalling
b	0.3	4.9	1041.9	0.7	outgoing
c	0.5	27.8	190.8	0.8	outgoing
d1	1.0	55.2	108.4	1.3	outgoing
d2	1.0	50.6	115.2	1.2	infalling
d3	1.0	4.7	1086.2	0.7	infalling

model (Gregory & Thomson 1984, Beers et al. 1992). Several solutions could explain the observed dynamics of A3921 allowing both the pre-merging and the post-merging cases (Ferrari et al. 2005); they are summarised in Table 3.

A comparison with the X-ray properties of the cluster is at this point essential to discriminate between the possible merging scenarios. The analysis of XMM-Newton observations by Belsole et al. (2005) reveals that the X-ray emission of A3921-A can be modelled with a 2Dβ-model, leaving a distorted residual structure toward the NW, coincident with A3921-B (see Fig. 4). The main cluster detected in X-rays is centred on the BCG position (BG1), while the X-ray peak of the NW clump is offset from the brightest galaxy of A3921-B (BG2) (see Belsole et al. 2005). The temperature map of the cluster shows an extended hot region oriented parallel to the line joining the centres of the two sub-clusters. A comparison of this image with numerical simulations by Ricker & Sarazin (2001) suggests that we are observing the central phases of an off-axis merger between two unequal mass objects, with clump A being the more massive component (Belsole et al. 2005), consistent with optical results.

By combining the signatures of merging derived both from the optical iso-density map and from X-ray results, we have then reconsidered the solutions of the two-body dynamical model summarised in Table 3 (Ferrari et al. 2005). In the pre-merger case, the high-angle solutions of cases (a1) and (a2) would imply a very large real separation of the two sub-clusters ($\sim 6-7$ Mpc), which is very unlikely taking into account the clear signs of interaction between the two clumps observed both in the optical and in X-rays. In the "recent" post-merger case, we can also exclude the solution (c), as we expect a higher value of the relative velocity ($\geq$1000 km/s) between the two clumps for obtaining so clearly a hot bar in the temperature map. Finally, the comparison of observed and simulated galaxy density and temperature maps (e.g. Schindler & Böhringer 1993, Ricker & Sarazin 2001) clearly exclude an older merger (e.g. t_0=1 Gyr), as we would not expect to observe a clear bimodal morphology in the optical any longer and we should not detect such obvious structure in the temperature map. Therefore, only the solutions corresponding to the very central phases of merging ($t_0 \approx \pm 0.3$ Gyr) can explain all our observational results, implying a collision axis nearly perpendicular to the line of sight. This is consistent with the absence of strong merging signatures in the observed projected velocity distribution of cluster members.

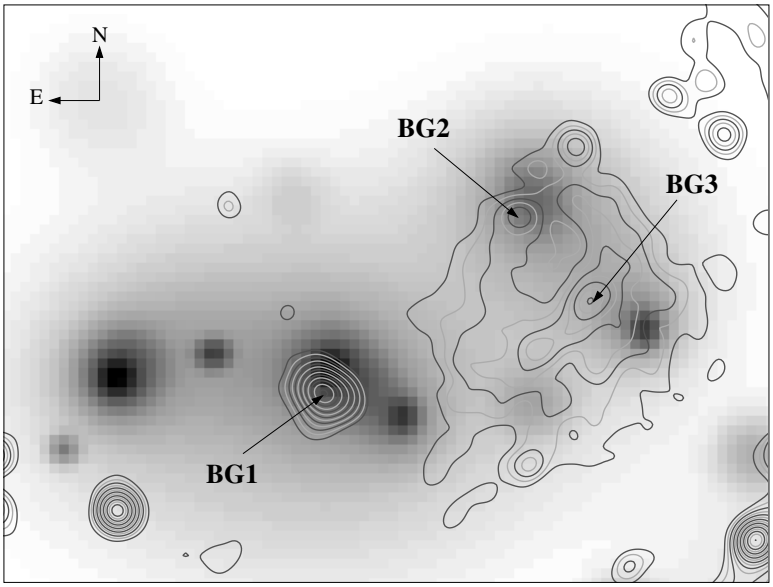

Figure 4: X-ray residuals after subtraction of a 2D-β model (Belsole et al. 2005) overlaid on the red sequence galaxy density map of the central part of A3921 ($22 \times 18\mathrm{arcmin}^2$, Ferrari et al. 2005).

The superposition of the X-ray residuals onto the optical iso-density map (Fig. 4) shows that the bulk of X-ray emission in A3921-B is offset towards SW from the main concentration of galaxies. As numerical simulations show that the non-collisio-

nal component is much less affected by the collision than the gas distribution (e.g. Röttiger et al. 1993), this offset suggests that A3921-B is tangentially traversing A3921-A in the SW/NE direction, with its galaxies in advance with respect to the gaseous component. The off-axis collision geometry has probably prevented total assimilation of the B group into the main cluster A. This off-axis collision scenario is also consistent with the shape of the feature in the temperature map (Belsole et al. 2005).

3.2 The effects of the merging event on star formation

3.2.1 Identification of the active galaxies in A3921

The next step of our work has been the identification of the active cluster members to study their possible link with the dynamical state of A3921. Various methods have been suggested for this purpose, using generally the presence and strength of the [OII] (λ=3727 Å) line and of Balmer lines (typically one or a combination of H_δ, H_γ, and H_β lines). In principle, as shown by Newberry et al. (1990), the most robust approach to detect post-star-burst galaxies would make full use of all three Balmer lines. However, our limited spectral range does not allow to include H_β in numerous cases, and the S/N ratio of the H_γ line is generally poor. Therefore, we have used the combination of [OII] and of the H_δ line to establish our spectral classification, as in Dressler et al. (1999).

For measuring the equivalent widths of these lines, we have used a Gaussian fitting technique through the task "splot" in IRAF. The equivalent widths of absorption and emission features are defined as positive and negative respectively, and the minimum measurable EW of each spectrum, estimated as in Barrena et al. (2002), is of ~ 2.8 Å.

We have identified the following active galaxies:

- 11 star-forming galaxies, characterised by the presence of emission lines, that have been divided into three categories (spiral-like spectra, star-bursts and probable dusty star-bursts), as described in section 2.1.1;

- 6 k+a's or post-star-burst galaxies, characterised, following the definition of Dressler et al. (1999), by absent [OII] emission and moderately strong Balmer absorption (3 Å$< \mathrm{EW}(\mathrm{H}_\delta) <$ 8 Å);

- 7 k+a candidates (k+a?), that do not strictly follow the criterion of Dressler et al. (1999), but present a clear inversion of the intensities of the K and H calcium lines. Since this is due to the presence of a blend of the H line with the Balmer line $\mathrm{H}\epsilon$, these objects have probably undergone a recent star-formation activity (Rose 1985).

The percentages of star-forming and post-star-forming galaxies (13% and 16% of the identified cluster members) are comparable to higher redshift clusters. Since several studies do not detect significant recent SF in low-redshift clusters (e.g. Dressler et al. 2004), the high fraction of active galaxies detected in A3921 is already an

important results in itself, which suggests a possible link between the SF properties of this cluster and its dynamical state.

3.2.2 Is the recent SF due to the merging event?

In order to understand if the presence of recent or on-going star-forming galaxies is related to the merging event detected in A3921, we have compared the spatial and velocity distributions of the active and passive cluster members (Figs. 5 and 6). The colour and spectral properties of active galaxies have also been taken into account.

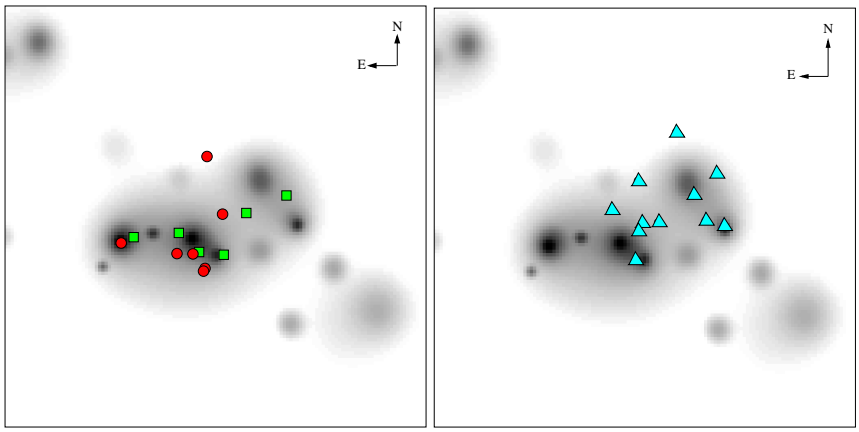

Figure 5: *Projected galaxy density map (34×34* arcmin^2*) of the red-sequence galaxies with* $R_{\mathrm{AB}} < 19$. **Left:** *the squares represent galaxies that are members of A3921 and classified as k+a and the circles as "k+a?" (see text).* **Right:** *the triangles show the location of emission line cluster member galaxies (Ferrari et al. 2005).*

The typical EW(Hδ) of the k+a/k+a? galaxies detected in A3921 is moderate and most of the objects have red colours, indistinguishable from red-sequence objects. We fail to detect the population of blue k+a with strong Balmer lines as detected in Coma by Poggianti et al. (2004), which can only be reproduced by a star-burst in the recent past. In contrast, our objects reflect the evolution of galaxies having undergone star-burst or star-forming activity which has been suppressed by some physical process, and now are in the second half of their lifetime (typically < 1.5 Gyr), with redder colours, and fainter Balmer lines, before reaching a k-type spectrum. This population can be reproduced by simply halting continuous star formation, without evoking a strong star burst. The k+a? objects are probably galaxies that have undergone a still older and fainter last episode of star formation, as they do not have Balmer lines strong enough to enter the k+a sample, but show clear signatures of past activity. Moreover, k+a/k+a? galaxies are mostly distributed over the main cluster A, and they do not show a spatial correlation with the region of the cluster mostly affected by the merging event.

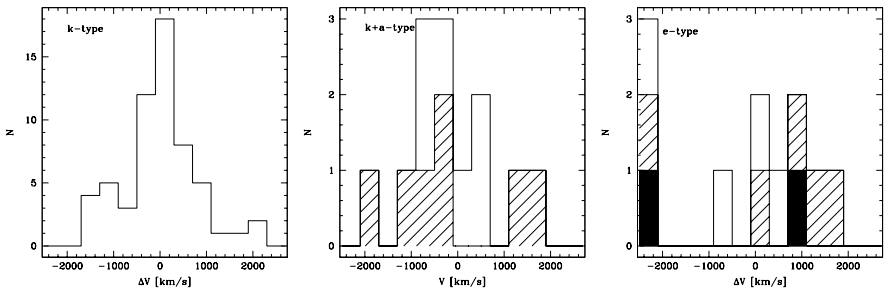

Figure 6: From left to right, velocity distribution (with a binning of 400 km/s) of k, k+a and emission line galaxies. In the central figure, the white component corresponds to secure k+a's and the shaded part to k+a candidates. In the right panel, the shaded component of the histogram corresponds to e(a)'s, the black component to e(b)'s, the white boxes to e(c) type objects (Ferrari et al. 2005).

On the contrary, most of the emission line galaxies lie in the region of the sub-cluster B, and in the region in between A and B. A similar spatial distribution is shown by blue galaxies, which are more clustered in the central region of A3921-B than in the whole field and, in particular, than in the centre of the more massive clump A (see Fig. 7). The comparison of the observed distributions of blue and emission line objects with the merging scenario presented previously ($\pm$ 0.3 Gyr) suggests that the interaction with the ICM during the passage of the sub-cluster B on the edge of cluster A may have triggered star-bursting. This hypothesis is supported by the significant difference in the radial velocity dispersions of emission-line and passive galaxies, suggesting that emission-line objects are a dynamically younger population than the general cluster members. In contrast, the k+a/k+a? population shows the signature of older star formation activity which can hardly be related to the on-going merger, but may be understood either as previously infalling galaxies, or is a relic from another older merging process, but is now at rest within the main cluster, as shown from the velocity distribution.

We therefore conclude that, in the case of A3921, the on-going merger may have triggered a star-formation episode in at least a fraction of the observed emission-line galaxies.

3.3 On-going follow-up

We are currently going on with the programme by observational and numerical analysis of A3921. Combined narrow-band H_α imaging (WFI@ESO 2.2m), high sensitivity radio observations (ATCA) and 2dF spectroscopy including the H_α region of the spectrum will reveal in a complementary way the active population in the central field of A3921 ($\sim 30' \times 30'$), identifying in addition the dusty star-burst galaxies previously missed due to [OII] extinction (see Sect. 2.1.1). Moreover, since both the 2dF and the ATCA observations cover a wider region of the cluster (1.5×1.5 deg^2),

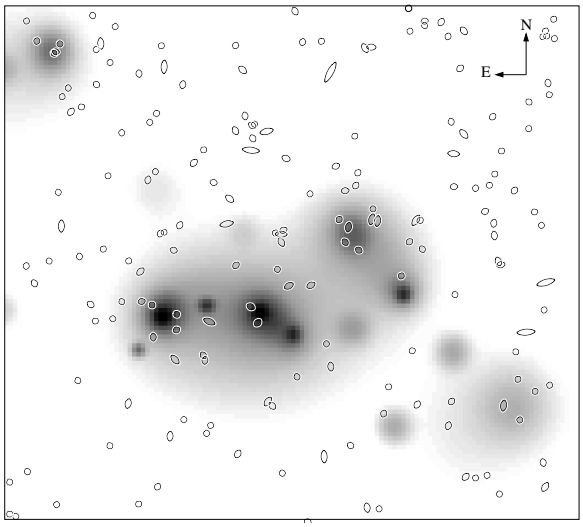

Figure 7: Projected galaxy density map (34×34 arcmin^2) of the red-sequence galaxies. The symbols represent the galaxies with $R_{\mathrm{AB}} < 20$ and bluer than the red sequence galaxies.

it will be possible to study the dynamics and the SF properties of the cluster out to its virial radius. Finally, we are currently analysing a Chandra observation of this cluster, which will give us high resolution density, temperature and metallicity maps of the ICM, essential to understand the link between the gas compression and the SF episode in active galaxies. These observations will allow us to test and eventually constrain better the previously found link between the merging event and the SFR of cluster members.

Our observational analysis will be finally compared with the numerical simulations performed by Schindler and collaborators. At present, we are working on modelling A3921, in order to refine the merging scenario reconstructed from the observational results. Our second step will be the comparison of the observed SF properties and metallicity maps of A3921 to the results of simulations. This will be an essential step to study in detail the physical effects acting on cluster members and affecting their SFR.

Acknowledgements. I warmly thank all my collaborators working on a) the optical (Christophe Benoist, Alberto Cappi, Sophie Maurogordato and Eric Slezak), X-ray (Elena Belsole, Hervé Bourdin, Gabriel W. Pratt and Jean-Luc Sauvageot) and radio (Luigina Feretti and Dick Hunstead) analysis of A3921, and b) the numerical simulations of merging clusters (Willfreid Domainko, Wolfgang Kapferer, Stefan Kimerswenger, Thomas Kronberger, Magdalena Mair, Sabine Schindler, Eelco van Kampen). This research is supported by a Marie Curie individual fellowship MEIF-CT-2003-900773.

References

Arnaud, M., Maurogordato, S., Slezak, E., Rho, J. 2000, A&A, 355, 461

Baldi, A., Bardelli, S., Zucca, E. 2001, MNRAS, 324, 509

Barrena, R., Biviano, A., Ramella, M., Falco, E.E., Seitz, S. 2002, A&A, 386, 861

Bartholomew, L. J., Rose, J. A., Gaba, A. E., Caldwell, N. 2001, AJ, 122, 2913

Bekki, K., Couch, W. J., Shioya, Y. 2002, ApJ, 577, 651

Bekki, K., Shioya, Y, Couch, W. J. 2001, ApJL, 547, 17

Bekki, K. 1999, ApJL, 510, 15

Belsole, E., Sauvageot, J.-L., Pratt, G. W. , Bourdin, H. 2005, A&A, 430, 385

Beers, T. C., Gebhardt, K., Huchra, J.P., Forman, W., Jones, C., Bothun, G. D. 1992, ApJ, 400, 410

Beers, T. C., Flynn, K., Gebhardt, K. 1990, AJ, 100, 32

Bird, C. M., & Beers, T. C. 1993, AJ, 105, 1596

Blake, C., Pracy, M., Couch, W. et al. 2005, MNRAS, 355, 713

Borgani, S., Murante, G., Springel, V., Diaferio, A., Dolag, K., Moscardini, L., Tormen, G., Tornatore, L., Tozzi, P. 2004, MNRAS, 348, 1078

Butcher, H., Oemler, A. 1978, ApJ, 219, 18

Davis, D. S., Bird, C. M., Mushotzky, R. F., Odewahn, S. C. 1995, ApJ, 440, 48

De Young, D.S. 1978, ApJ, 223, 47

Domainko, W., Kapferer, W., Schindler, S., van Kampen, E., Kimeswenger, S., Mair, M., Ruffert, M. 2004, proceeding of the XXXIXth Rencontres de Moriond "Exploring the Universe", La Thuile (28.03.-04.04.2004), astro-ph/0405577

Donnelly, R., Forman, W., Jones, C., Quintana, H., Ramirez, A., Churazov, E., Gilfanov, M. 2001, ApJ, 562, 254

Dressler, A., Oemler, A., Poggianti, B., Smail, I., Trager, S., Shectman, S. A., Couch, W., Ellis, R. 2004, ApJ, 617, 867

Dressler, A., Gunn, J. E. 1983, ApJ, 270, 7

Dressler A., Smail, I., Poggianti, B. M., Butcher, H., Couch, W. J., Ellis, R. S., Oemler, A. 1999, ApJ, 122, 51

Durret, F., Forman, W., Gerbal, D., Jones, C., Vikhlinin, A. 1998, A&A, 335, 41

Evrard, A. E. 1991, MNRAS, 248, 8

Fadda, D., Slezak, E., Bijaoui, A. 1998, A&AS, 127, 335

Ferrari, C., Benoist, C., Maurogordato, S., Cappi, A., Slezak, E. 2005, A&A, 430, 19

Ferrari, C., Maurogordato, S., Cappi, A., Benoist, C. 2003, A&A, 399, 813

Fujita, Y., Takizawa, M., Nagashima, M., Enoki, M. 1999, PASJ, 51, L1

Gomez, P., Nichol, R., Miller, C., Goto, T. 2001, AAS, 199.7801

Gregory, S. A., Thompson, L. A. 1984, ApJ, 286, 422

Kapferer, W., Breitschwerdt, D., Domainko, W., Schindler, S., van Kampen, E., Kimeswenger, S., Mair, M. 2004, proceeding of the XXXIXth Rencontres de Moriond "Exploring the Universe", La Thuile (28.03.-04.04.2004), astro-ph/0405577

Larson, R. B., Tinsley, B. M., Caldwell, C. N. 1980, ApJ, 237, 692

Lavery, R. J., Henry, J. P. 1988 ApJ, 330, 596

Lemonon, L., Pierre, M., Hunstead, R., Reid, A., Mellier, Y., Böhringer, H. 1997, A&A, 326, 34

Maurogordato, S., Proust, D., Beers, T. C., Arnaud, M., Pellò, R., Cappi, A., Slezak, E., Kriessler, J. R. 2000, A&A, 355, 848

McLachlan, G. J., Basford, K. E. 1988, Mixture Models (Marcel Dekker, New York)

Miller, N. A., Owen, F. N. 2001, ApJ, 554, 25

Moore, B., Katz, N., Lake, G. 1996, ApJ, 457, 455

Newberry, M. V., Boronson, T. A., Kirshner, R. P. 1990, ApJ, 350, 585

Poggianti, B. M., Bridges, T. J., Komiyama, Y., Yagi, M., Carter, D., Mobasher, B., Okamura, S., Kashikawa, N. 2004, ApJ, 601, 197

Poggianti, B. M., Smail, I., Dressler, A., Couch, W. J., Barger, A. J., Butcher, H., Ellis, R. S., Oemler, A. 1999, ApJ, 518, 576

Quilis, V., Moore, B., Bower, R. 2000, SCIENCE, 288, 1617

Ricker, P. M., Sarazin, C. L. 2001, ApJ, 561, 621

Rose, J. A. 1985, AJ, 90, 1927

Röttiger, K., Stone, J. M., Mushotzky, R. F. 1998, ApJ, 493, 62

Röttiger, K., Burns, J., Loken, C. 1993, ApJL, 407, 53

Sarazin, C. L. 2003, Physics of Plasmas, 10, 1992

Sarazin, C. L. 2001, ApJ, 561, 621

Sarazin, C. L. 1988, "X-ray Emission from Clusters of Galaxies," (Cambridge: Cambridge University Press)

Schindler, S., Böhringer, H. 1993, A&A, 269, 83

Schindler, S., Müller, E. 1993, A&A, 272, 137

Struck, C. 1999, Physics Report, 1999, 321,1

Tomita, A., Nakamura, F. E., Takata, T., Nakanishi, K., Takeuchi, T., Ohta, K., Yamada, T. 1996, AJ, 111, 42

van Kampen, E., Jimenez, R., Peacock, J. A. 1999, MNRAS, 310, 43

Zabludoff, A. I., Zaritsky, D., Lin, H., Tucker, D., Hashimoto, Y., Shectman, S. A., Oemler, A., Kirshner, R. P. 1996, ApJ, 466, 104